

**COMMENTS ON FREQUENCY SWEEPED ROTATING INPUT PERTURBATION TECHNIQUES
AND IDENTIFICATION OF THE FLUID FORCE MODELS IN ROTOR/
BEARING/SEAL SYSTEMS AND FLUID HANDLING MACHINES**

Agnes Muszynska and Donald E. Bently
Bentley Rotor Dynamics Research Corporation
Minden, Nevada 89423, U.S.A.

The paper describes perturbation techniques used for identification of rotating system dynamic characteristics. A comparison between two periodic frequency-swept perturbation methods applied in identification of fluid forces of rotating machines is presented. The description of the fluid force model identified by inputting circular periodic frequency-swept force is given. This model is based on the existence and strength of the circumferential flow, most often generated by the shaft rotation. The application of the fluid force model in rotor dynamic analysis is presented. It is shown that the rotor stability is an entire rotating system property. Some areas for further research are discussed.

1. INTRODUCTION

Perturbation methodology is well known and widely applied in Control Theory. The main objective of perturbation is identification of the system characteristics by exciting the system with a known input function and observing (measuring) its response. The comparison between the input and output of the system gives an insight into the system characteristics, i.e., its transfer function (Fig. 1). The "system" can be a mechanical structure, or any other system, such as biological, economic, etc. When little is known about the system characteristics, the system is often referred to as a "black box." When the mathematical structure of the system characteristics is known (or rather assumed approximately known, such as, for instance linearity of the n-th order), the system is referred to as a "grey box." The identification procedure provides the parameters to the assumed mathematical structure of the system model. The transition from a "black box" to "grey box" is performed by iterative adjustments to the system model. It results from a series of perturbation tests conducted for various operating conditions.

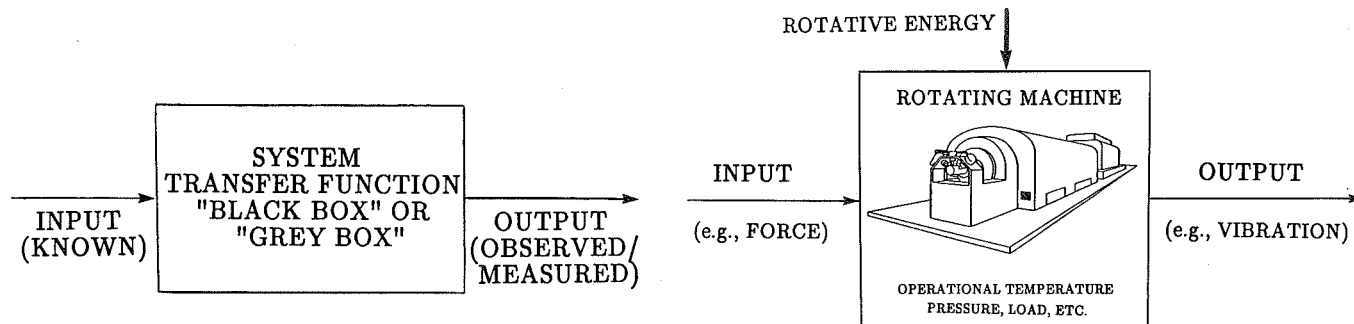


Figure 1. - Identification of object characteristics by comparison of the input and output.

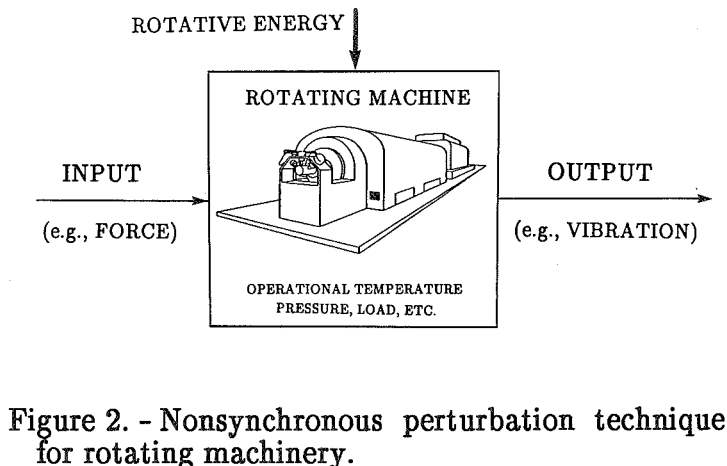


Figure 2. - Nonsynchronous perturbation technique for rotating machinery.

1.1 Perturbation Techniques in Rotating Machinery

Rotating machines are particular subjects of perturbation testing. They represent a special class of "active" mechanical structures. The main motion of a rotating machine is rotation, driven by an external energy source. In order to fully understand the rotating machine process, and identify its operational characteristics, the perturbation tests should be conducted on a machine at its operational conditions, in particular when the rotor rotates at its operating speed (Fig. 2). The rotative energy provides, therefore, an additional input to the system. Most often this input is considered uncoupled from the perturbation input/output flow. The rotating energy, as an additional input to the system has, however, a very important influence on the system: its characteristics become rotative speed dependent. The perturbation input should be entirely independent from the rotative energy input. This technique is called "nonsynchronous" perturbation [1].

There are two particular cases of the perturbation technique applied to rotating machinery. In these cases only one input is used: (i) perturbation of the rotating machine at rest (like a "passive" structure), and (ii) synchronous perturbation. In the latter technique the rotative energy represents the only input to the system. In the synchronous perturbation method a controlled unbalance transfers rotational energy into an input force [2,3]. Both these particular perturbation techniques often provide important, but also very limited, information about the rotating machine characteristics.

1.2 Characteristics of Rotating Machines

Perturbation testing of rotating machines is used for identification of their mechanical characteristics associated with modes of vibration. Shaft lateral/ bending modes attract the highest attention. In particular, the lowest lateral/ bending modes are of the greatest concern because, due to the specific role of internal damping in rotating systems, they are usually characterized by the highest vibration amplitudes, thus creating conditions for rotor failures.

In most rotating machines the shaft rotates in a fluid environment. Fluid involved in dynamic motion becomes an important part of the system. Fluid/solid interaction causes the appearance of additional modes of vibration in the system. These particular modes have been identified by nonsynchronous perturbation testing [1]. Perturbation testing is used for identification of the rotating machine characteristics at various conditions such as under steady-state or variable load, unbalance, at different rotative speeds, including operational speed and above, at various temperatures, and other conditions. The information provided from the perturbation testing is used for model adjustments; it helps to predict stability of machine operation, provides tools for malfunction diagnostics, and assists in optimization of the machine performance.

1.3 Perturbation Input

Rotating machines can be perturbed by all classical input functions used in the identification of mechanical structures. Frequency swept periodic inputs [4–27], random inputs [28], and impulse inputs [29–35] became the most popular ones. Provided that the identified system is linear, all perturbation methods should lead to the same results. Each method has, however, its own strong and weak points which result in accuracy differences in specific applications. Two methods of nonsynchronous perturbation which have several advantages in comparison with other techniques are discussed below.

1.4 Comparison of Two Frequency Swept Rotating Input Perturbation Techniques Used for Identification of Fluid Forces in Rotating Machines

There are two main perturbation techniques of nonsynchronous one-mode testing used for identification of fluid force models in rotor/bearing, rotor/seal systems, as well as in fluid handling

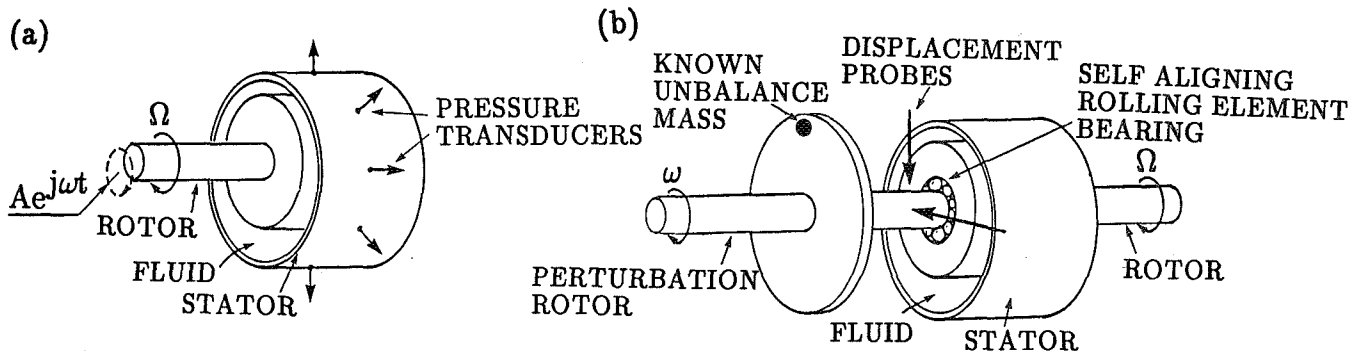


Figure 3. - Nonsynchronous perturbation techniques: (a) perturbation by displacement (a stationary shaft and casing displacements are also used), (b) perturbation by force.

machines (mainly pumps). The basic advantage of these methods is the rotational character of the input function in forward or reverse direction (the same or opposite to rotor rotation). This allows for independent identification of forward and backward modes of the rotating machine. These two perturbation techniques differ by the input/output functions (Fig. 3). For rotor circular orbits* they are as follows:

$$\text{DISPLACEMENT: } Ae^{j\omega t} \rightarrow \boxed{\bar{\kappa}(\omega) = \frac{1}{\bar{H}(\omega)}} \text{ FORCE: } (F_r + jF_t)e^{j\omega t} \rightarrow [\text{Refs. 7,11,12,18-26}]$$

$$\text{FORCE: } Fe^{j\omega t} \rightarrow \boxed{\bar{H}(\omega) = \frac{1}{\bar{\kappa}(\omega)}} \text{ DISPLACEMENT: } Ae^{j(\omega t + \alpha)} \rightarrow [\text{Refs. 4-6,8-10,13-17}]$$

where A is rotor displacement amplitude, α is rotor response phase (also $\alpha = \arctan(-F_t/F_r)$), ω is rotor perturbation (excitation) precessional frequency (usually varying from zero to some ω_{\max}), t is time, $j = \sqrt{-1}$, F_r and F_t are radial and tangential forces respectively acting on the rotor. These forces are obtained by integrating the fluid pressure or measuring forces outside an elastically supported seal or bearing; F is the input force amplitude.

In both cases the objective is identification of the "black box," i.e., the transfer function of the system. More precisely the sought functions are $\bar{\kappa}(\omega)$ = complex dynamic stiffness, or $\bar{H}(\omega) = \frac{1}{\bar{\kappa}(\omega)}$ = transfer function = complex dynamic compliance of the system. The most often obtained result from either technique is the complex dynamic stiffness:

$$\bar{\kappa}(\omega) = \frac{F_r + jF_t}{A} \text{ when the input is displacement.} \quad (1)$$

$$\bar{\kappa}(\omega) = \frac{F}{A} e^{-j\alpha} \text{ when the input is force.} \quad (2)$$

*A use of noncircular forces/displacements or occurrences of noncircular response orbits/forces represent generalizations of the perturbation method, useful for higher eccentricities of the rotor [13]. For full identification of system parameters it requires a double number of measurements.

The complex dynamic stiffness components are as follows:

$$\text{Direct dynamic stiffness} \equiv \text{DDS} = \frac{F_r}{A} = \frac{F \cos \alpha}{A} \quad (3)$$

$$\text{Quadrature dynamic stiffness} \equiv \text{QDS} = \frac{F_t}{A} = -\frac{F \sin \alpha}{A} \quad (4)$$

By limiting the input to a circular periodic function, both methodologies must yield exactly the same results, provided that the system is linear, and the instrumentation yields comparable signal-to-noise ratios.

As is evident from Eqs. (3) and (4), the force-to-motion amplitude ratios F_r/A and F_t/A correspond to the direct and quadrature dynamic stiffnesses, respectively, often, in some published papers, with opposite sign convention. The authors use the notion of dynamic stiffnesses, well established in Mechanics. For a system with one complex degree of freedom (one lateral mode of the symmetric rotor with no gyroscopic effect) the Direct dynamic stiffness is composed of the static (direct) stiffness (K), minus the effect of inertia and cross damping. By definition, the static stiffness K is positive; therefore, it appears in the direct dynamic stiffness with the plus sign. The quadrature dynamic stiffness contains the product of the radial (direct) damping (D) and frequency ω , minus the constant (perturbation frequency independent) cross coupled stiffness. Since damping is positive, it is reasonable to present the corresponding straight line $D\omega$ versus perturbation frequency with a positive slope. The data from Refs. [21–23] illustrated in figures below have been presented in this unified format. The elements of the discussed above dynamic stiffnesses correspond to the standard linear bearing or seal models with isotropic properties (fluid inertia matrix with no cross terms, damping, and stiffness matrices skew symmetric).

The results of perturbation testing of rotor/fluid systems are discussed in the next section.

2. FLUID FORCE MODEL IDENTIFIED BY INPUTTING CIRCULAR PERIODIC FREQUENCY SWEPT FORCE

As a result of over eight years of testing and identification research, the authors have proposed a fluid force model for lightly loaded bearings, seals, and fluid-handling machines, based on the significance of the steady circumferential flow [36]. The model was identified experimentally mainly by using the frequency swept circular periodic perturbation force at the input of the rotor/bearing/seal systems. A similar fluid force model was previously developed theoretically, and has existed in a simplified version in the rotordynamic literature for at least 25 years (Bolotin [37], Black [38,39]). It has not, however, been fully exploited. Following the results of the perturbation testing, the most important improvement in the model introduced by the authors was the replacement of the constant "1/2," widely used in the fluid models, by the factor " λ " (fluid circumferential average velocity ratio) as a function of fluid parameters and shaft eccentricity. This ratio has been identified for several cases of seals and bearings as a decreasing function of shaft eccentricity.

The basic fluid circumferential average velocity ratio λ is generated by the shaft rotation. Its value can, however, be strongly modified by forced fluid flow, such as preswirling and injections. Depending on the direction of the tangential preswirls and/or injections, λ can be reduced when these directions oppose shaft rotation, or increased when the preswirls/injections are in the direction of shaft rotation.

For an originally concentric shaft rotating at a constant rotative speed Ω and perturbed by an unbalanced auxiliary system providing the frequency swept rotating force with frequency ω in a range at least covering the interval $0 < \omega < \Omega$ for the "whirl" mode, the plot of direct dynamic stiffness of the fluid dynamic effects (shaft and other mechanical effects excluded), versus perturbation frequency ω approximately forms a parabola (Figs. 4 and 5), and thus can be described by three parameters. By using circular input forces and maintaining isotropy of the system (rotor gravity load balanced by centering springs), so that the response orbits are circular, the authors identified the fluid force direct dynamic stiffness as [1]:

$$DDS = K_0 - M_f(\omega - \lambda\Omega)^2 \tag{5}$$

where K_0 is the fluid film static radial (direct) stiffness, M_f is the fluid inertia effect, and λ is the fluid circumferential average velocity ratio. Note that the "cross damping" (skew-symmetric terms in the damping matrix) appears in (5) as a function of the fluid inertia and Coriolis' acceleration.

The quadrature dynamic stiffness versus perturbation frequency usually forms a straight line (Figs. 6 and 7); thus, it can be described by two parameters. The authors have identified these parameters as

$$QDS = D(\omega - \lambda\Omega) \tag{6}$$

where D is the fluid film radial (direct) damping. The term $D\omega$ represents the passive effect of the shaft pushing the fluid, $-D\lambda\Omega$ is an active term transferring rotative energy into the fluid force pulling the shaft (tangential force). The quadrature dynamic stiffness (6) is the most representative and most important part of the fluid force model [40]. In spite of nonlinearities of both λ and D as functions of shaft eccentricity, QDS appears as a distinctly straight line for all tested cases except for high shaft eccentricity [1,13]. This also means that there is practically no cross inertia effect in the fluid force. Note that in the identified fluid force model the direct and quadrature dynamic stiffnesses carry the common factor λ . This means that the peak of DDS and zero of QDS occur at the same perturbation frequency (Figs. 5 and 7). The results obtained by other researchers show, however, some differences in frequency for these values (Figs. 4 and 6). This problem will be discussed in Section 7.

Figures 4 to 7 illustrate the basic results obtained by various researchers, by using nonsynchronous perturbation techniques.

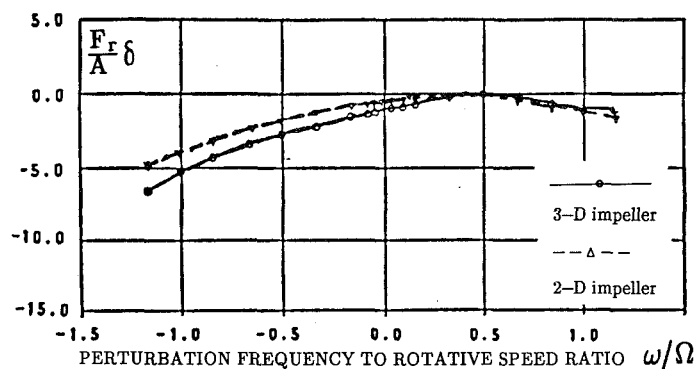


Figure 4. - Direct Dynamic Stiffness versus perturbation frequency for the system with circular displacement input, and force output. δ denotes a nondimensionalizing coefficient. Courtesy of H. Ohashi [22].

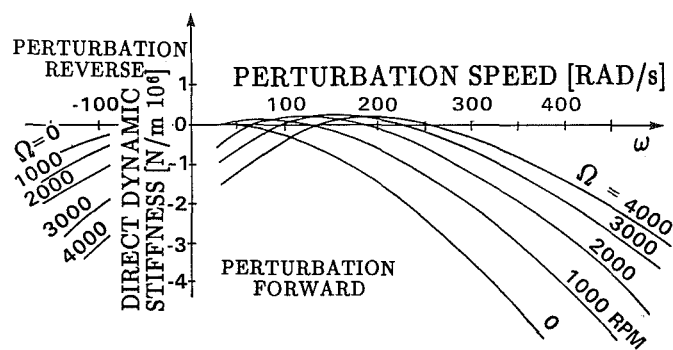


Figure 5. - Direct Dynamic Stiffness versus perturbation frequency for the system with circular force input, and displacement output [10].

The original response vectors versus perturbation frequency are presented in Figs. 8 and 9, in the form of Bodé plots. Note that, in the technique which uses force input, the displacement response vector has a form characteristic of responses for a one-mode system to a periodic excitation with sweep frequency (Fig. 9). The occurrence of a resonance is obvious. In comparison with the response of a classical mechanical system, the response phase is, however, ahead of the

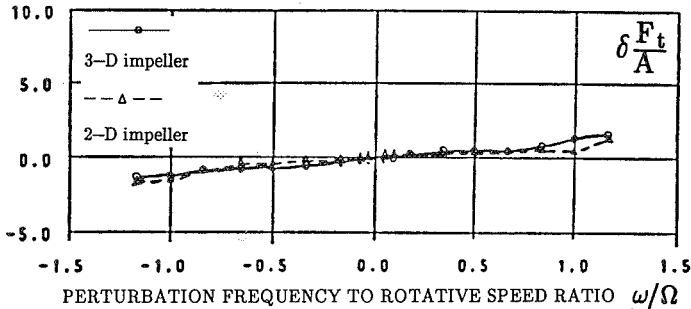


Figure 6. - Quadrature Dynamic Stiffness versus perturbation frequency for the system with circular displacement input, and force output. δ denotes a nondimensionalizing coefficient. Courtesy of H. Ohashi [22].

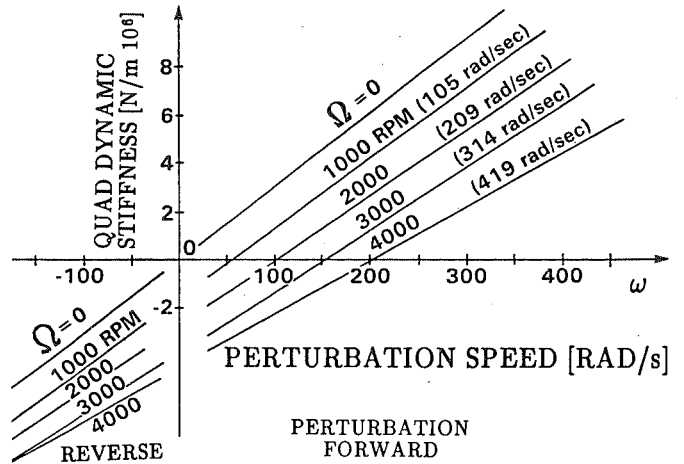


Figure 7. - Quadrature Dynamic Stiffness versus perturbation frequency for the system with circular force input, and displacement output [10].

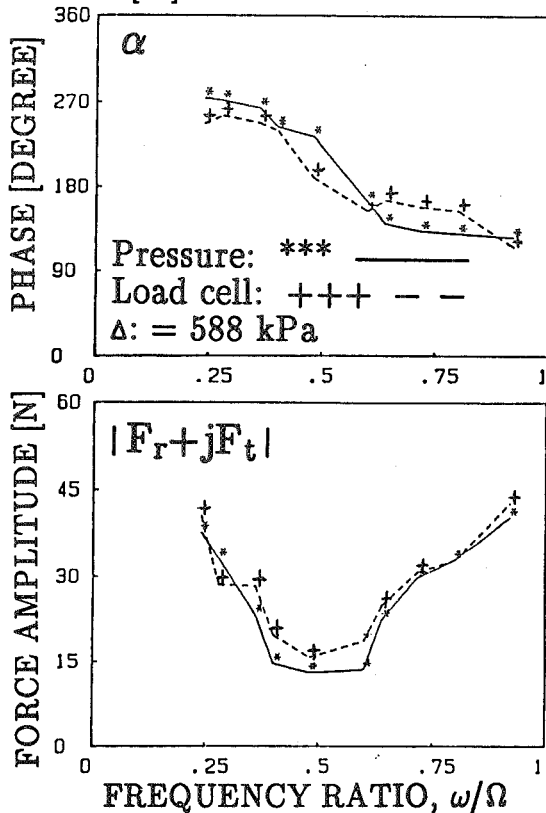


Figure 8. - Force response phase and amplitude versus perturbation frequency (perturbation by displacement. Courtesy of T. Iwatsubo [23].

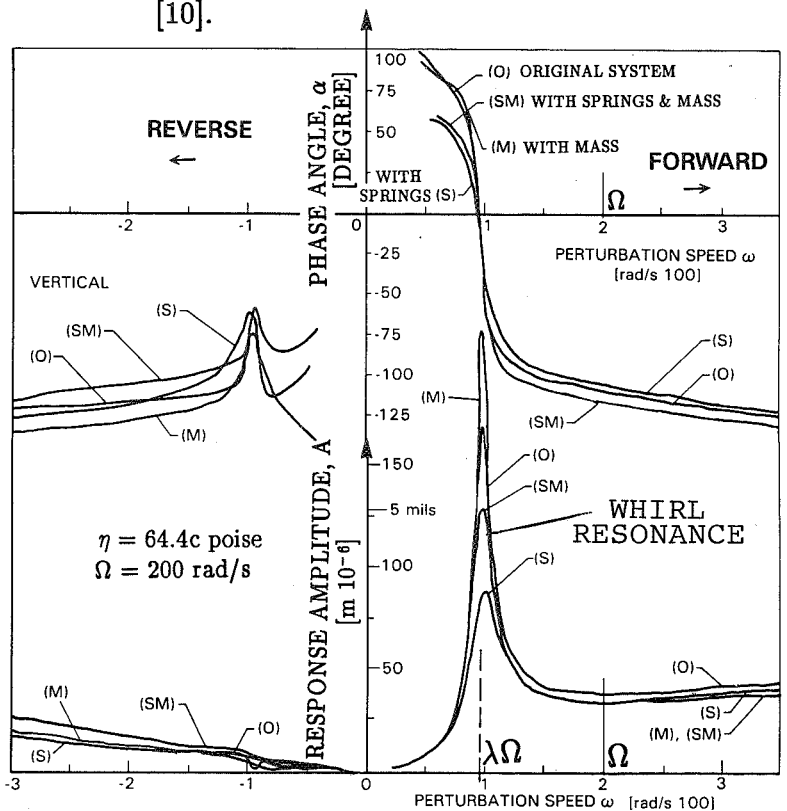


Figure 9. - Displacement response phase and amplitude versus perturbation frequency (perturbation by force) [9].

input force, and the phase sharply drops around 0° . This indicates the "quadrature" nature of this particular resonant phenomenon. The resonant frequency occurs at about $\lambda\Omega$, where Ω is the rotative speed. This means that $\lambda\Omega$ represents one of the system natural frequencies, which is generated purely by the fluid/solid interaction. The system QDS becomes zero. This fluid-related quadrature resonance was documented by Stone & Underwood in 1947 [4], and again by Hull in 1955 [5], but these excellent works were not immediately pursued. When the force is used as the system input, as opposed to a displacement input, the physical interpretation of the results becomes clear. The peak amplitude, which occurs when the quadrature dynamic stiffness equals zero, is of course limited by the total direct stiffness term in exactly the same fashion as the resonance at the zero of the direct stiffness, (yielding the classical stiffness-over-mass-related natural frequency) is limited by the total quadrature stiffness term (classical damping). The peak amplitudes may become very high, if the shaft rotative speed approaches the $1/\lambda$ value of the rotor system "mechanical" natural frequency, corresponding to its first bending mode [16]. (Note that the responses include rotor mechanical effects.) In fact, instability occurs when both direct and quadrature dynamic stiffnesses zero at the same frequency. This subject is discussed in Section 5.

By inputting a constant circular displacement and measuring the output in terms of forces, not only the accuracy of the results is lower, but also there is no clear physical interpretation of the results. The plot of force response amplitude versus perturbation frequency has an "anti-resonance" shape, a concave curve, a mirror image of displacement response amplitude versus frequency (Fig. 8). The phase is exactly the same in both techniques. It is obvious: by definition, the phase represents the angle between the input vector and output vector, independent of the nature of the input and output functions. Note that the dip point of the response force amplitude occurs around one half of the rotative speed, i.e., the fluid circumferential average velocity ratio λ is close to $1/2$. The notion of the "force resonance," or rather "anti-resonance" is not well known in Mechanics. That is why by using the input force methodology, the authors have been more fortunate than those who used forces as outputs, to see direct physical interpretation of the results, namely that the value close to $\lambda\Omega$ is a system natural frequency.

Note the advantage of the circular perturbation, as opposed to unilateral perturbation as in impulse testing. The results of forward perturbation (rotation and precession in the same direction) and backward perturbation (opposed direction) are significantly different (Fig. 9). The resonance occurs only for the forward perturbation, i.e., the "quadrature" natural frequency $\lambda\Omega$ of the system has the plus sign only (classical "direct" natural frequencies governed by stiffness and mass have + and - signs).

3. FLUID FORCE MODEL IN DIFFERENTIAL FORM

In more general terms, the identified fluid force model can be presented as follows. In the coordinate system which rotates at an angular velocity $\lambda\Omega$ the fluid force is assumed radial, with three components (Fig. 10):

$$\text{Fluid force in rotating coordinates} = M_f \ddot{z}_r + D \dot{z}_r + K_0 z_r \quad (7)$$

where $z_r(t) = x_r(t) + jy_r(t)$ are the shaft lateral displacements in rotating coordinates; M_f , D and K_0 are the fluid inertia effect, damping and stiffness respectively.

The coordinate transformation

$$z_r = z e^{-j\lambda\Omega t}, \quad \text{where } z(t) = x(t) + jy(t), \quad j = \sqrt{-1} \quad (8)$$

from rotating $z_r(t)$ to stationary coordinates $z(t)$ yields the fluid force:

$$\text{Fluid force in stationary coordinates} = M_f(\ddot{z} - 2j\lambda\Omega\dot{z} - \lambda^2\Omega^2z) + D(\dot{z} - j\lambda\Omega z) + K_0z \quad (9)$$

The fluid force model, in differential form (9), can be directly used in rotor dynamic analyses. In particular, for shaft periodic circular motion with a constant amplitude:

$$z = Ae^{j\omega t} \quad (10)$$

$$\begin{aligned} \text{Fluid force for periodic motion} &= A\{-M_f(\omega - \lambda\Omega)^2 + jD(\omega - \lambda\Omega) + K_0\}e^{j\omega t} \equiv \\ &\equiv Ae^{j\omega t} \{DDS + jQDS\} \equiv Ae^{j\omega t} \{\bar{\kappa}(\omega)\} \end{aligned} \quad (11)$$

where $\bar{\kappa}(\omega)$ is the previously discussed complex dynamic stiffness.

4. IDENTIFICATION OF THE NONLINEAR MODEL

While determining the appropriate interpretation and use of the direct stiffness basic parabola, and the quadrature stiffness straight line, the authors are also investigating situations where the dynamic stiffness components diverge from parabolic and straight line shapes (Figs. 11 to 13). These are cases of nonlinearities, and discontinuous shifts of various basic parameters. An example is shown below.

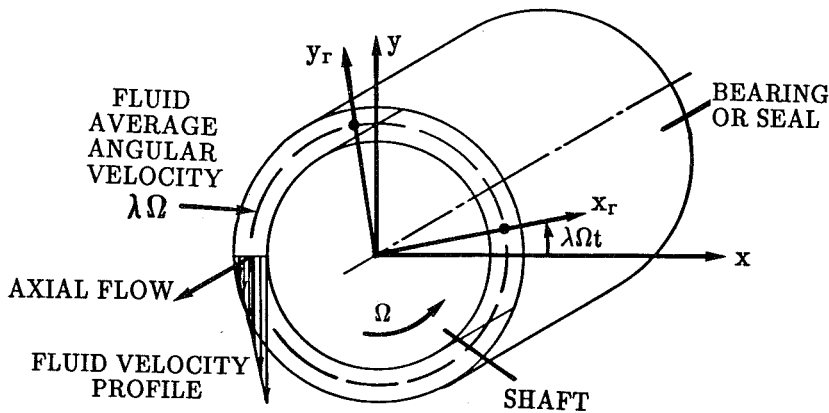


Figure 10. - Fluid force model for lightly loaded shaft.

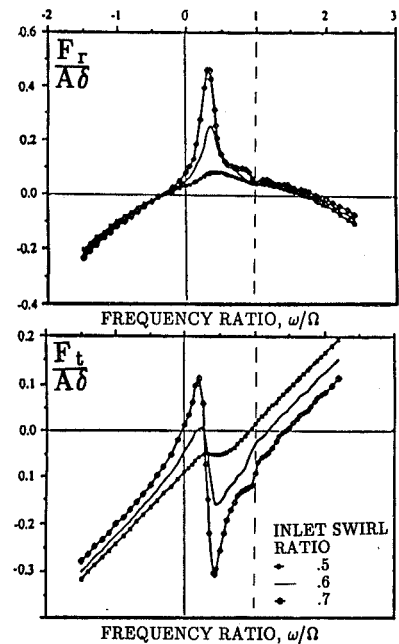


Figure 11. - Direct and Quadrature Dynamic Stiffnesses with nonlinear effects (perturbation by displacement). δ denotes a nondimensionalizing coefficient. Courtesy of D. Childs [21].

By inputting a force with sufficiently high amplitude $F = mr\omega^2$ (m, r are mass and radius of a controlled unbalance), the response becomes modified by system nonlinearities. The resulting dynamic stiffnesses diverge slightly from the parabolic/straight line shapes (Figs. 12 and 13). This occurs most noticeably in the range of perturbation frequency where the response amplitude is the largest (around $\omega = \lambda\Omega$) (Fig. 9). By inputting forces with sequentially increasing amplitudes, F , for each consecutive test, the nonlinear functions in the fluid force model can be identified. This identification technique is graphically presented in Fig. 14. As a first step the DDS for a linear case (when F is small) is subtracted from the DDS for a nonlinear case. The result gives the stiffness nonlinear function ψ versus perturbation frequency. Using this relationship, as well as the response amplitude versus perturbation frequency for high F , the plot of ψ versus shaft eccentricity can be

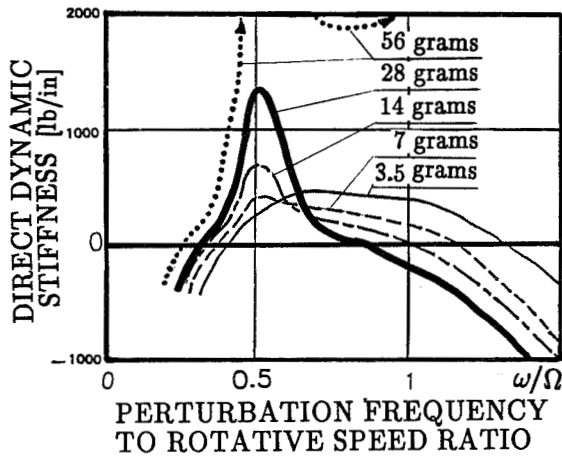


Figure 12. - Direct Dynamic Stiffnesses with nonlinear effects (perturbation by force for several cases of unbalance masses) [14].

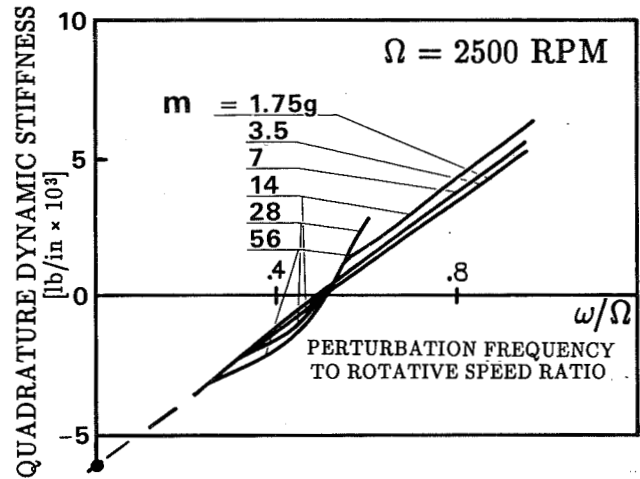


Figure 13. - Quadrature Dynamic Stiffness with nonlinear effects (perturbation by force) [17]. m denotes mass of perturbation unbalance.

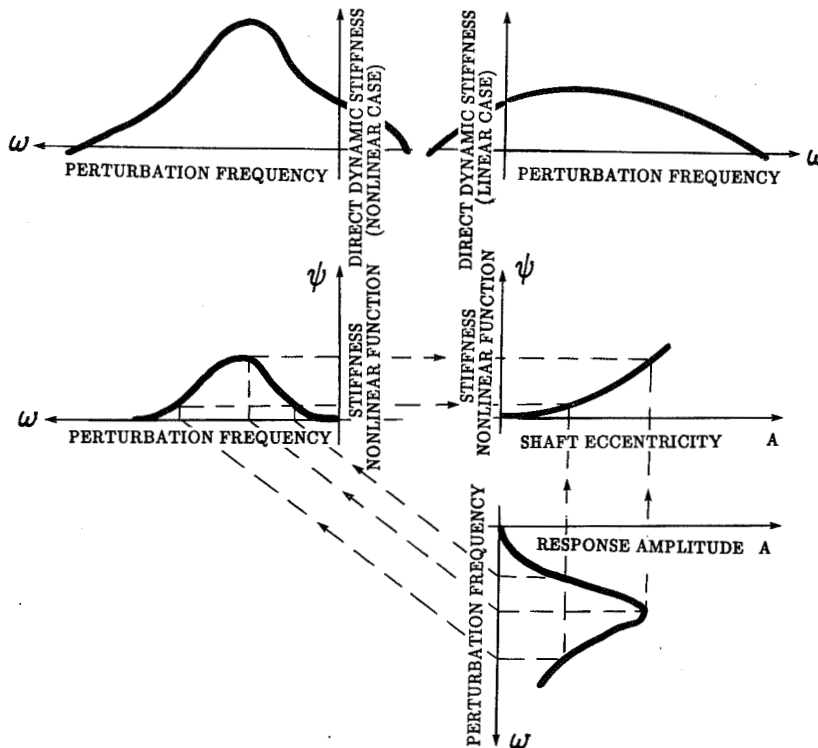


Figure 14. - Identification of fluid film stiffness nonlinearity (perturbation by force).

obtained. Note that the response amplitude A represents a rotating radial eccentricity of the shaft. Assuming lateral symmetry, the rotating eccentricity corresponds to the unidirectional static eccentricity of the rotor.

By a very similar method, the fluid film radial damping nonlinearity can be identified from the quadrature dynamic stiffness, provided that the nonlinearity of λ is relatively small [17].

Note that the nonlinear effects in the fluid film may be caused and/or influenced by fluid injections and preswirls [21], as well as cavitations [26].

5. ROTOR STABILITY: CRITERION AND MARGINS OF STABILITY

The rotor/fluid system dynamic stiffness components as functions of perturbation frequency can be used to predict the rotor stability and the stability margin.

In very general terms, the threshold of stability occurs when the "zeros" of the direct and quadrature dynamic stiffnesses occur at the same perturbation/precession frequency. In terms of frequency, the stability margin is the lowest difference between the zeros of the direct and quadrature dynamic stiffnesses (Fig. 15).

In actual applications, both components of the fluid force dynamic stiffness become modified by the rotor system parameters. An example is discussed below.

Consider an isotropic rotor supported in one rigid and one fluid-lubricated bearing (Fig. 16). The rotor rotates at a constant speed Ω and is perturbed by a nonsynchronous periodic circular forward (in the direction of rotation) sweep frequency force $Fe^{j\omega t}$. The model of the system is as follows:

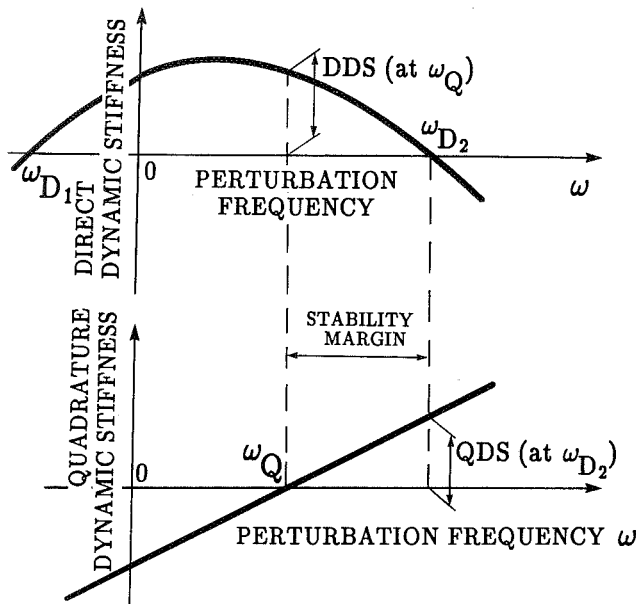


Figure 15. - Rotor stability prediction using dynamic stiffness graphs.

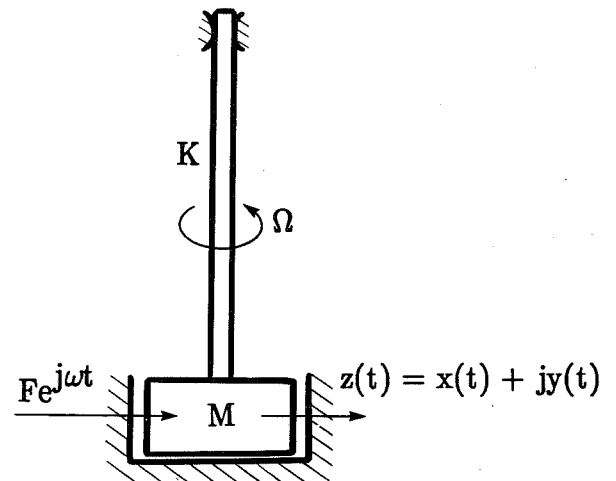


Figure 16. - Rotor/bearing system model.

$$M\ddot{z} + M_f(\ddot{z} - 2j\lambda\Omega\dot{z} - \lambda^2\Omega^2z) + D_s\dot{z} + D(\dot{z} - j\lambda\Omega z) + Kz + K_0z = Fe^{j\omega t} \quad (12)$$

where M , D_s , K are rotor generalized (modal) mass, damping, and stiffness, for the first lateral mode respectively. The rotor system response is circular:

$$z = Ae^{j(\omega t + \alpha)} \quad (13)$$

where the amplitude A and phase α can be calculated when Eq. (13) is substituted in Eq. (12):

$$Ae^{j\alpha}[-M\omega^2 - M_f(\omega - \lambda\Omega)^2 + D_s j\omega + D j(\omega - \lambda\Omega) + K + K_0] = F \quad (14)$$

From Eq. (14) the amplitude A and phase α of the forced response (13) are obtained as follows:

$$A = \frac{F}{\sqrt{[K + K_0 - M\omega^2 - M_f(\omega - \lambda\Omega)^2]^2 + [D_s\omega + D(\omega - \lambda\Omega)]^2}} \quad (15)$$

$$\alpha = \arctan \frac{D_s\omega + D(\omega - \lambda\Omega)}{M\omega^2 + M_f(\omega - \lambda\Omega)^2 - K - K_0} \quad (16)$$

The whirl resonance (Fig. 9) occurs when the quadrature part of the denominator of Eq. (15) is equal to zero, i.e., when

$$\omega = \frac{\lambda\Omega}{1 + D_s/D} \equiv \omega_{\text{res}} \quad (17)$$

The resonant amplitude and phase are

$$A_{\text{res}} = \frac{F}{|K + K_0 - (M + M_f D_s^2/D^2)\lambda^2\Omega^2/(1 + D_s/D)^2|} \approx \frac{F}{|K + K_0 - M\lambda^2\Omega^2|}, \quad \alpha_{\text{res}} = 0$$

The actual peak amplitude depends, however, on whether the force amplitude F is constant or dependent on frequency ω .

Eq. (16) indicates the leading-phase phenomenon for low frequency. At $\omega = 0$ the phase is

$$\alpha = \arctan \frac{D\lambda\Omega}{K + K_0} > 0$$

For $\lambda\Omega > 0$ the response is, therefore, ahead of the exciting force.

Eqs. (15) and (16) also show clearly that the whirl resonance occurs only if Ω and ω have the same rotational directions (perturbation forward). If $\omega < 0$ (perturbation backward), then the quadrature resonance does not take place (compare with experimental results, Fig. 9).

The system complex dynamic stiffness is obtained from Eq. (14) as the ratio $F/(Ae^{j\alpha})$. The dynamic stiffness components are

$$\text{DDS} = -M\omega^2 - M_f(\omega - \lambda\Omega)^2 + K + K_0 \quad (18)$$

$$\text{QDS} = D_s\omega + D(\omega - \lambda\Omega) \quad (19)$$

The system dynamic stiffness is, therefore, a combination of the rotor and fluid-related terms.

The eigenvalue problem for Eq. (12) provides the following eigenvalues:

$$s_{1,2,3,4} = \frac{1}{2(M+M_f)} (-D-D_s + 2j\lambda\Omega M_f) \pm \frac{1}{\sqrt{2}} \left[\sqrt{-P + \sqrt{P^2 + R^2}} \pm j\sqrt{P + \sqrt{P^2 + R^2}} \right]$$

where

$$P = \frac{K+K_0 - M_f\lambda^2\Omega^2}{M+M_f} - \left[\frac{D+D_s}{2(M+M_f)} \right]^2 + \left[\frac{\lambda\Omega M_f}{M+M_f} \right]^2, \quad R = \left[\frac{M_f(D+D_s)}{(M+M_f)^2} - \frac{D}{M+M_f} \right] \lambda\Omega$$

The stability criterion, i.e., the requirement that all eigenvalues have non-positive real parts is as follows:

$$-\frac{D+D_s}{2(M+M_f)} + \frac{1}{\sqrt{2}} \sqrt{-P + \sqrt{P^2 + R^2}} \leq 0 \quad (20)$$

which yields the rotative speed threshold of stability:

$$\Omega \leq \frac{1}{\lambda} \left[1 + \frac{D_s}{D} \right] \sqrt{\frac{K+K_0}{M+M_f} \frac{D^2}{D_s^2}}$$

The natural frequency at the threshold of stability is $\sqrt{\frac{K+K_0}{M+M_f} \frac{D^2}{D_s^2}}$ (this is the imaginary part of the eigenvalue).

Inequality (20) can also be solved in another form:

$$\frac{\lambda\Omega}{1+M/M_f} - \sqrt{\frac{K+K_0}{M+M_f} - \lambda^2\Omega^2 \frac{MM_f}{(M+M_f)^2}} \leq \frac{\lambda\Omega}{1+D_s/D} \leq \frac{\lambda\Omega}{1+M/M_f} + \sqrt{\frac{K+K_0}{M+M_f} - \lambda^2\Omega^2 \frac{MM_f}{(M+M_f)^2}} \quad (21)$$

The direct dynamic stiffness (18) is equal to zero when

$$\omega = \omega_{D1,2} \equiv \frac{\lambda\Omega}{1+M/M_f} \pm \sqrt{\frac{K+K_0}{M+M_f} - \lambda^2\Omega^2 \frac{MM_f}{(M+M_f)^2}} \quad (22)$$

The values $\omega_{D1,2}$ are called roots (zeros) of the direct dynamic stiffness. The quadrature dynamic stiffness (19) is equal to zero when

$$\omega = \omega_Q \equiv \frac{\lambda\Omega}{1+D_s/D} \quad (23)$$

where ω_Q is the root (zero) of the quadrature dynamic stiffness. The stability criterion (21) can, therefore, be written as

$$\omega_{D1} \leq \omega_Q \leq \omega_{D2}$$

which means, for rotor stability, the root of the system quadrature dynamic stiffness should occur between the two roots of the direct dynamic stiffness.

The margin of stability, in terms of frequency, is defined as a minimum distance between roots:

$$\min[(\omega_Q - \omega_{D1}), (\omega_{D2} - \omega_Q)] \quad (24)$$

This margin of stability is "horizontal," thus expressed in terms of frequency (Fig. 15). An additional "vertical" margin of stability can also be defined. It expresses the direct and quadrature dynamic stiffness closeness to the threshold of stability (Fig. 15):

$$\min [DDS(\text{at } \omega_Q), QDS(\text{at } \omega_{D1}), QDS(\text{at } \omega_{D2})] \quad (25)$$

The stability margin (25) indicates which parameter of the system is most likely responsible for the instability.

The threshold of stability occurs when both direct and quadrature dynamic stiffness have the same root, i.e., either $\omega_{D1} = \omega_Q$ or $\omega_Q = \omega_{D2}$. It means that at the precession frequency when these equalities occur, the total complex dynamic stiffness of the system equals zero (see Eq. (15) in which the denominator is zero at this case).

When the threshold of stability is exceeded, the vibration amplitude increases, most often ending up in a limit cycle self-excited vibrations, known as "whirl" and "whip," which are governed by the system nonlinearities [40, 41].

The fluid force model presented in the dynamic stiffness form provides clear suggestions for stability improvements of rotor/bearing/seal systems. Higher stability margins result when

- λ decreases (provided that $DM > D_s M_f$, which is almost always satisfied)
- K_0 increases
- D decreases (most often is, however, insensitive to stability)
- M_f decreases
- K and D_s increase
- M decreases

A higher stability margin results also when the rotative speed Ω decreases. Since variations of Ω can involve other rotor dynamic effects, such as balance resonance which may interact with fluid effects [40], Ω is not included in the above list.

The most effective parameters for rotor stability control are a decrease of the fluid circumferential velocity ratio λ and an increase of the fluid film radial stiffness K_0 . The first is widely known in "anti-swirl" applications [41-51]. The second, i.e., the increase of K_0 results directly from an increase of shaft eccentricity and/or increase of the fluid pressure. The latter conclusion applies to externally pressurized ("hydrostatic") bearing and seal designs, which are widely known for their stability features. The most surprising result concerns fluid radial damping D . In most cases, an increase of D has no influence on stability, or has even a minor negative

effect. (This effect can be compared to destabilizing action of rotor structural/ internal friction at high rotative speeds.)

An interesting result is obtained if the classical Half Power Bandwidth method is applied to the whirl resonance. The classical amplification factor Q may be calculated as

$$Q = \frac{\omega_{res}}{\omega_2 - \omega_1}$$

where ω_{res} is given by Eq. (17) and ω_1, ω_2 are frequencies corresponding to the phases equal to $\pm 45^\circ$ or amplitudes at $A_{res}/\sqrt{2}$ (3 dB level). For the whirl resonance the amplification becomes (Fig. 9):

$$Q \approx \frac{\sqrt{(K+K_0)M}}{D} \frac{1}{\sqrt{(K+K_0)/M} / \lambda \Omega - 1} \quad (26)$$

The first fraction of Eq. (26) is the classical relationship of half the inverse of the damping factor. The second fraction indicates the closeness of the direct resonance (zero of DDS) to quadrature resonance. (Shaft damping and fluid inertia effect were omitted in Eq. (26) for clarity.) The whirl resonant amplitude becomes significantly magnified if the rotative speed is close to $1/\lambda$ times the rotor lateral mode natural frequency. This effect has often been observed experimentally [16].

Finally, the dynamic stiffness format can be used to successfully predict rotor instability in case of nonlinear distortions of the basic parabola/straight lines. The general idea always holds true: Instability occurs when both DDS and QDS have zeros at the same perturbation/precession frequency. Nonlinear effects may cause dramatic changes in the shape of DDS and/or QDS, including multiple zero points. Theoretical studies [52] proved, for instance, that the low frequency rotating stall instability can be predicted using the method discussed above.

Note that the relationships discussed in this chapter hold true for the considered example of one mode isotropic rotor/bearing or rotor/seal system. When more modes are taken into account, the relationships become more complex.

6. APPLICATIONS OF THE FLUID FORCE MODEL

By implementing the model identified by the authors into rotating machine dynamic equations, several significant and valuable results were obtained. The results of analysis conducted for one, two, and three mode models of rotors are very encouraging [36,40,41,42,53,54]. The model allowed for explanation of new phenomena, such as the recently observed second mode whirl [53] and second mode whip [54]. The generalization from two and three modes to "n" modes is obvious [53]. All swirl preventive measures (such as anti-swirl, preswirl, swirl brakes, fluid injections) can also be easily included in the models [41,42], and thus would give designers very good insight into the expected efficiency of such devices for stability of rotating machines.

7. FLUID FORCE MODEL ADJUSTMENTS AND GENERALIZATIONS

The model of fluid force (9) identified by the authors, using force input perturbation testing, is certainly open to further developments. One adjustment, namely the addition of nonlinear terms,

was discussed in Section 4. There exist also some other possible modifications to the model. These include:

(i) Tangential components. In the original form (7), the fluid force was assumed to have radial components only. There is a high probability, especially when the shaft eccentricity increases, that the force components are not exactly radial, but also have a tangential part. For instance the stiffness force in (7) may require an addition: the term $K_0 z_r$ should be replaced by $(K_0 - jK_t)z_r$ where K_t is tangential stiffness.

(ii) Two fluid circumferential velocity ratios. In the model (7), it was assumed that all components of the fluid force rotate at the same angular velocity $\lambda\Omega$. It might be necessary to introduce two different ratios λ_1, λ_2 , one for the fluid inertia force, the other for the damping force. Thus, the adjusted model (9) will contain the terms:

$$M_f(\ddot{z} - 2j\lambda_1\Omega\dot{z} - \lambda_1^2\Omega^2z) + D(\dot{z} - j\lambda_2\Omega z)$$

where $\lambda_1\Omega$ and $\lambda_2\Omega$ are angular velocities at which inertia and damping forces rotate correspondingly. Two different λ ratios seem to be required in order to adequately identify the fluid force model in pumps (see Figs. 4 and 6 [22]).

(iii) Higher order terms. Some results of perturbation testing [26] suggest that the fluid force contains terms of order higher than two. In particular a third order term (jerk) should be included. With an assumed additional value of the corresponding fluid circumferential velocity ratio, λ_3 , the model (9) might, therefore, be completed by the following term:

$$J(\ddot{z} - 3j\lambda_3\Omega\dot{z} - 3\lambda_3^2\Omega^2z + j\lambda_3^3\Omega^3z)$$

where J can be considered as a complex parameter, containing radial and tangential components.

(iv) Nonsymmetric fluid force. Most results of the perturbation testing have been obtained for symmetric cases: perturbation around the shaft centered position. When the shaft is statically displaced to higher eccentricity, the flow conditions are certainly modified. The fluid force then contains terms of nonsymmetric nature [13,14]. In particular, the nonlinear terms identified for symmetric cases as simple functions of radial eccentricity, may require adjustments. More research is required in this area.

8. CONCLUDING REMARKS

This paper discusses the use of nonsynchronous swept frequency harmonic rotating input perturbation techniques for identification of the fluid force model in lightly loaded rotor/bearing/seal systems. Two basic methods differ by a choice of input functions: either as a force, as used by the authors and a few other researchers [1,2,4-6,8-10,13-17], or as a displacement [7,11,12,18-26]. The measured output responses are displacements or forces respectively. While both methods provide the system dynamic stiffness characteristics, the main difference between these two methods consists in data generation, acquisition, and processing; thus they provide different levels of signal-to-noise ratios. A significant contributor to noise is input/output phase readings. The first method provides a higher accuracy (around $\pm 0.3\%$) than the second method, especially in phase measurements. An estimated error of the first method final results is lower than $\pm 3\%$. An application of both methods to the same system (if possible) might ultimately provide the best identification data.

The results, in terms of the system dynamic stiffness components obtained from both methods, are very similar, as should be expected. Based on results of hundreds of tests obtained over the past eight years, the authors have provided a consistent mechanical interpretation of the results, and proposed an improved model of fluid forces in lightly loaded bearings and seals [36]. The model includes the fluid circumferential average velocity ratio as a function of shaft eccentricity, instead of a constant value 1/2 as in the classical models. (In some recent analyses the assumption about the constant 1/2 ratio starts gradually fading away.) The bearing/seal coefficients can easily be obtained from the proposed model as particular cases. The application of the improved fluid force model in rotor/bearing/seal systems yields results which stand in a very good agreement with observed and documented dynamic phenomena, such as whirl, whip, and higher mode whirl/whip vibrations [36,40,41,53,54]. The model allows for an improved prediction of the rotor stability thresholds and stability margins, as well as quantifying stability control measures. Some possible further adjustments of the fluid force model are also discussed. The latter would require more, well coordinated, experimental research.

The database resulting from different types of perturbation methodologies applied to rotor/bearing/seal/pump systems is now quite rich, including data from CalTech, Mitsubishi, Sulzer Brothers Ltd., Universities of Kobe, Tokyo, Osaka, Kaiserslautern, Texas A&M, and Case Western. It will be very useful to reduce the acquired experimental, as well as analytical/numerical, data in the form proposed in [55]. It will then become clearer what adjustments the model would require. It will also indicate directions for further research.

REFERENCES

1. Muszynska, A.: Modal Testing of Rotor/Bearing Systems, *The International Journal of Analytical and Experimental Modal Analysis*, July 1986, pp. 15-34.
2. Bently, D. E.; Muszynska, A. and Jones, D. I. G.: Some Aspects of the Application of Mechanical Impedance for Turbomachinery and Structural System Parameter Identification, *Proc. of 3rd International Modal Analysis Conference*, Orlando, Florida, January 1985, pp. 177-186.
3. Childs, D. W. and Kim, Chang-Ho: Testing for Rotordynamic Coefficients and Leakage: Circumferentially-grooved Turbulent Annular Seals, *The International Conference on Rotordynamics*, Tokyo, Japan, September 1986, pp. 609-618.
4. Stone, J. M. and Underwood, F. A.: Load Carrying Capacity of Journal Bearings, *SAE Quart. Trans.*, No. 1, 1947.
5. Hull, E. H.: Journal Bearing Behavior Under Periodic Loading, G.I. Research Laboratory, Rep. No. 55-RL-1354, Schenectady, New York, 1955.
6. Bently, D. E. and Bosmans, R. F.: Oil Whirl Resonance, *Fundamentals of the Design of Fluid Film Bearings*, Published by ASME, 1979, pp. 131-193.
7. Iwatsubo, T.: Evaluation of Instability Forces of Labyrinth Seals in Turbines or Compressors, *Rotordynamic Instability Problems in High-Performance Turbomachinery*, NASA CP 2133, The First Texas A&M University Workshop, College Station, Texas, May 1980, pp. 139-168.

8. Bently, D. E. and Muszynska, A.: Stability Evaluation of Rotor/Bearing System by Perturbation Tests, Rotor Dynamic Instability Problems in High Performance Turbomachinery, NASA CP 2250, The Second Workshop at Texas A&M University, College Station, Texas, 1982, pp. 307-322.
9. Bently, D. E. and Muszynska, A.: Oil Whirl Identification by Perturbation Test, Advances in Computer-Aided Bearing Design, 82-72978, ASME/ASLE Lubrication Conference, Washington, D.C., October 1982, pp. 111-119.
10. Bently, D. E. and Muszynska, A.: Perturbation Tests of Bearing/Seal for Evaluation of Dynamic Coefficients, Symposium on Rotor Dynamical Instability, Summer Annual Conference of the ASME Applied Mechanics Division, AMD — Vol. 55, Houston, Texas, June 1983, pp. 75-88.
11. Ohashi, H. and Shoji, H.: Lateral Fluid Forces Acting on a Whirling Centrifugal Impeller in Vaneless and Vaned Diffuser, Rotordynamic Instability Problems in High-Performance Turbomachinery, NASA CP 2338, The Third Texas A&M University Workshop, College Station, Texas, May 1984, pp. 109-122.
12. Jery, B.; Acosta, A. J.; Brennen, C. E. and Caughey, T. K.: Hydrodynamic Impeller Stiffness, Damping, and Inertia, *ibid.*, pp. 137-160.
13. Bently, D. E. and Muszynska, A.: The Dynamic Stiffness Characteristics of High Eccentricity Ratio Bearings and Seals by Perturbation Testing, *ibid.*, pp. 481-491.
14. Bently, D. E. and Muszynska, A.: Identification of Bearing and Seal Dynamic Stiffness Parameters by Steady-State Load and Squeeze Film Tests, Proc. of BRDRC Symposium on Instability in Rotating Machinery, Carson City, Nevada, NASA CP 2409, 1985, pp. 301-316.
15. Bently, D. E. and Muszynska, A.: Measurement of Rotor System Dynamic Stiffness by Perturbation Testing, *ibid.*, pp. 47-58.
16. Bently, D. E. and Muszynska, A.: Perturbation Study of Rotor/Bearing System: Identification of the Oil Whirl and Oil Whip Resonances, Tenth Biennial ASME Design Engineering Division Conference on Mechanical Vibration and Noise, 85-DET-142, Cincinnati, Ohio, September 1985.
17. Bently, D. E. and Muszynska, A.: Modal Testing and Parameter Identification of Rotating Shaft/Fluid Lubricated Bearing System, Proc of the 4th International Modal Analysis Conference, Los Angeles, California, February 1986, pp. 1393-1402.
18. Adkins, D. R. and Brennen, C. E.: Origins of Hydrodynamic Forces on Centrifugal Pump Impellers, Rotordynamic Instability Problems in High-Performance Turbomachinery, NASA CP 2443, The Fourth Texas A&M University Workshop, NASA CP 2443, College Station, Texas, June 1986, pp. 467-492.
19. Childs, D. W.: Force and Moment Rotordynamic Coefficients for Pump-Impeller Shroud Surfaces, *ibid.*, pp. 503-530.
20. Kanki, H.; Fujii, H.; Hizume, A.; Ichimura, T. and Yamamoto, T.: Solving Nonsynchronous Vibration Problems of Large Rotating Machineries by Exciting Test in Actual Operating Condition, The International Conference on Rotordynamics, Tokyo, Japan, September 1986, pp. 221-226.

21. Childs, D. W.: Fluid-Structure Interaction Forces at Pump-Impeller-Shroud Surfaces for Rotordynamic Calculations, Rotating Machinery Dynamics, ASME DE-vol. 2, H0400B, Boston, Massachusetts, September 1987, pp. 581-594.
22. Ohashi, H.; Sakurai, A. and Nishihama, J.: Influence of Impeller and Diffuser Geometries on the Lateral Fluid Forces of Whirling Centrifugal Impeller, The Fifth Workshop on Rotordynamic Instability Problems in High Performance Turbomachinery, Texas A&M, NASA CP 3026, May 1988, pp. 285-306.
23. Iwatsubo, T.; Sheng, B. and Matsumoto, T.: An Experimental Study on the Static and Dynamic Characteristics of Pump Annular Seals, *ibid.*, pp. 229-252.
24. Childs, D. W.; Elrod, D. and Hale, K.: Annular Honeycomb Seals: Test Results for Leakage and Rotordynamic Coefficients, Comparison to Labyrinth and Smooth Configurations, *ibid.*, pp. 143-160.
25. Adams, M. L.; Yang, T. and Pace, S. E.: A Seal Test Facility for the Measurement of Isotropic and Anisotropic Linear Rotordynamic Characteristics, *ibid.*, pp. 253-268.
26. Brennen, C. E.; Franz, R. and Arndt, N.: Effects of Cavitation on Rotordynamic Force Matrices, 1988 Conference on Advanced Earth-to-Orbit Propulsion Technology, NASA, Huntsville, Alabama, May 1988, pp. 227-239.
27. Bolleter, U.; Wyss, A.; Welte, I. and Stürchler, R.: Measurement of Hydrodynamic Interaction Matrices of Boiler Feed Pump Impellers, *Trans. of the ASME, Journal of Vibration, Acoustics, Stress and Reliability in Design*, v. 109, April 1987.
28. Yasuda, C.; Kanki, H.; Ozawa, T. and Kawakami, T.: Application of Random Excitation Technique to Dynamic Characteristics Measurement of Bearing, The International Conference on Rotordynamics, Tokyo, Japan, September 1986, pp. 61-68.
29. Kanki, H.; Mori, S. and Hizume, A.: Theoretical and Experimental Study on the Destabilizing Force by Labyrinth Seal, *ibid.*, pp. 603-608.
30. Morton, P. G.: The Derivation of Bearing Characteristics by Means of Transient Excitation Applied Directly to a Rotating Shaft, *Dynamics of Rotors*, 1974 IUTAM Symposium, Lyngby, Denmark, Springer-Verlag, Berlin, Heidelberg, New York, 1975, pp. 350-379.
31. Nordmann, R. and Massman, H.: Identification of Dynamic Coefficients of Annular Turbulent Seals, Rotordynamic Instability Problems in High-Performance Turbomachinery, NASA CP 2338, The Third Texas A&M University Workshop, College Station, Texas, May 1984, pp. 294-312.
32. Massmann, H. and Nordmann, R.: Some New Results Concerning the Dynamic Behavior of Annular Turbulent Seals, *Instability in Rotating Machinery*, NASA CP 2409, Carson City, Nevada, 1985, pp. 179-194.
33. Nordmann, R.; Dietzen, F. J.; Janson, W.; Frei, A. and Florjancic, S.: Rotordynamic Coefficients and Leakage Flow for Smooth and Grooved Seals in Turbopumps, The International Conference on Rotordynamics, Tokyo, Japan, September 1986, pp. 619-628.
34. Nordmann, R. and Diewald, W.: Influence of Different Types of Seals on the Stability Behavior of Turbopumps, The Second International Symposium on Transport Phenomena, Dynamics and Design of Rotating Machinery, Honolulu, Hawaii, April 1988, pp. 351-361.

35. Diewald, W. and Nordmann, R.: Influence of Different Types of Seals on the Stability Behavior of Turbopumps, The Fifth Workshop on Rotordynamic Instability Problems in High-Performance Turbomachinery, Texas A&M University, College Station, Texas, NASA CP 3026, May 1988, pp. 197-210.
36. Muszynska, A.: Improvements in Lightly Loaded Rotor/Bearing and Rotor/Seal Models, Trans of the ASME Journal of Vibration Acoustics, Stress and Reliability in Design, v. 110, No. 2, April 1988, pp. 129-136.
37. Bolotin, V. V.: Nonconservative Problems in the Theory of Elastic Stability, The Macmillan Company, New York, 1963.
38. Black, H. F.: Effects of Hydraulic Forces in Annular Pressure Seals on the Vibrations of Centrifugal Pump Rotors, Journal of Mechanical Engineering Science, v. II, No. 2, 1969, pp. 206-213.
39. Black, H. F. and Jensen, D. N.: Dynamic Hybrid Bearing Characteristics of Annular Controlled Leakage Seals, Proceedings Journal of Mechanical Engineering, v. 184, 1970, pp. 92-100.
40. Muszynska, A.: Whirl and Whip — Rotor/Bearing Stability Problems, Journal of Sound and Vibration, v. 110, No. 3, 1986, pp. 443-462.
41. Muszynska, A. and Bently, D. E.: Anti-Swirl Arrangements Prevent Rotor/Seal Instability, Thermo-Fluid Dynamics of Rotating Machinery, Trans. of the ASME, Journal of Vibration, Acoustics, Stress and Reliability in Design, v. 111, April 1989, pp. 156-162.
42. Muszynska, A.; Franklin, W. D. and Bently, D. E.: Rotor Active "Anti-Swirl" Control, Trans of the ASME, Journal of Vibration, Acoustics, Stress and Reliability in Design, v. 110, No. 2, April 1988, pp. 143-150.
43. Jenny, R. and Wyssman, H. R.: Lateral Vibration Reduction in High Pressure Centrifugal Compressors, Proceedings of the 9th Turbomachinery Symposium, Texas A&M University, 1980, pp. 45-56.
44. Massey, I. C.: Subsynchronous Vibration Problems in High-Speed, Multistage Centrifugal Pumps, Proceedings of the 14th Turbomachinery Symposium, Texas A&M University, 1985.
45. Pace, S. E.; Florjancic, S. and Bolleter, U.: Rotordynamic Developments for High Speed Multistage Pumps, Proceedings of the 3rd International Pump Symposium, Texas A&M University, 1986.
46. Kirk, R. G. and Simpson, M.: Full Local Shop Testing of 1800 HP Gas Turbine Driven Centrifugal Compressor for Offshore Platform Service: Evaluation of Rotor Dynamics Performance, Proc. of Symp. Instability in Rotating Machinery, Carson City, Nevada, June 1985; NASA Conference Publication 2409, 1985, pp. 1-13.
47. Ambrosch, F. and Schwaebel, R.: Method of and Device for Avoiding Rotor Instability to Enhance Dynamic Power Limit of Turbines and Compressors, United States Patent, #4,273,510, June 1981.
48. Miller, E. H.: Rotor Stabilizing Labyrinth Seal for Steam Turbines, United States Patent #4,420,161, December 1983.

49. Wyssmann, H. R.: Theory and Measurements of Labyrinth Seal Coefficients for Rotor Stability of Turbocompressors, The Fourth Workshop on Rotordynamic Instability Problems in High Performance Turbomachinery, Texas A&M University, College Station, Texas, NASA CP 2443, June 1986, pp. 237–258.
50. Brown, R. D. and Leong, Y. M. M. S.: Experimental Measurements of Lateral Force in a Model Labyrinth and the Effect on Rotor Stability, The Third Workshop on Rotordynamic Instability Problems in High Performance Turbomachinery, NASA CP 2338, College Station, Texas, May 1989, pp. 187–210.
51. Brown, R. D. and Hart, A.: A Novel Form of Damper for Turbomachinery, The Fourth Workshop on Rotordynamic Instability Problems in High Performance Turbomachinery, Texas A&M University, College Station, Texas, June 1986, pp. 325–348.
52. Tsujimoto, Y.; Acosta, A. J. and Yoshida, Y.: A Theoretical Study of Fluid Forces on a Centrifugal Impeller Rotating and Whirling in a Varied Diffuser, The Fifth Workshop on Rotordynamic Instability Problems in High-Performance Turbomachinery, NASA CP 3026, Texas A&M, College Station, Texas, May 1988, pp. 307–322.
53. Muszynska, A.: Multi-Mode Whirl and Whip in Rotor/Bearing Systems, Dynamics of Rotating Machinery, Ed. by J. H. Kim and W. J. Yang, Hemisphere Publ. Corp., New York; Proc. of Second International Symposium on Transport Phenomena Dynamics, and Design in Rotating Machinery, Honolulu, Hawaii, April 1988, pp. 326–340.
54. Muszynska, A. and Grant, J. W.: Stability and Instability of a Two-Mode Rotor Supported by Two Fluid-Lubricated Bearings, BRDRC Report, No. 1/90, 1990.
55. Tam, L. T.; Przekwas, A. J.; Muszynska, A.; Hendricks, R. C.; Braun M. J. and Mullen R. L.: Numerical and Analytical Study of Fluid Dynamic Forces in Seals and Bearings, Rotating Machinery Dynamics, 1987 ASME Design Technology Conference, DE-vol. 2, 1987, Trans. of the ASME, Journal of Vibration, Acoustics, Stress, and Reliability in Design, v. 110, No. 3, July 1988, pp. 315–325.

NOTATION

A	Amplitude of rotor vibration
D, K_o, M_f	Fluid radial damping, stiffness, and inertia effect respectively
D_s, K, M	Rotor generalized (modal) damping, stiffness, and mass respectively
DDS, QDS	Direct and quadrature dynamic stiffness components respectively
F	Force amplitude
F_r, F_t	Radial and tangential force components
s	Eigenvalue
t	Time
$z = x + jy$	Rotor displacement in stationary coordinates
$z_r = x_r + jy_r$	Rotor displacement in rotating coordinates
α	Force/displacement phase
\bar{k}	Complex dynamic stiffness
λ	Fluid circumferential average velocity ratio
ω	Perturbation/precession frequency
Ω	Rotative speed